Additional examples

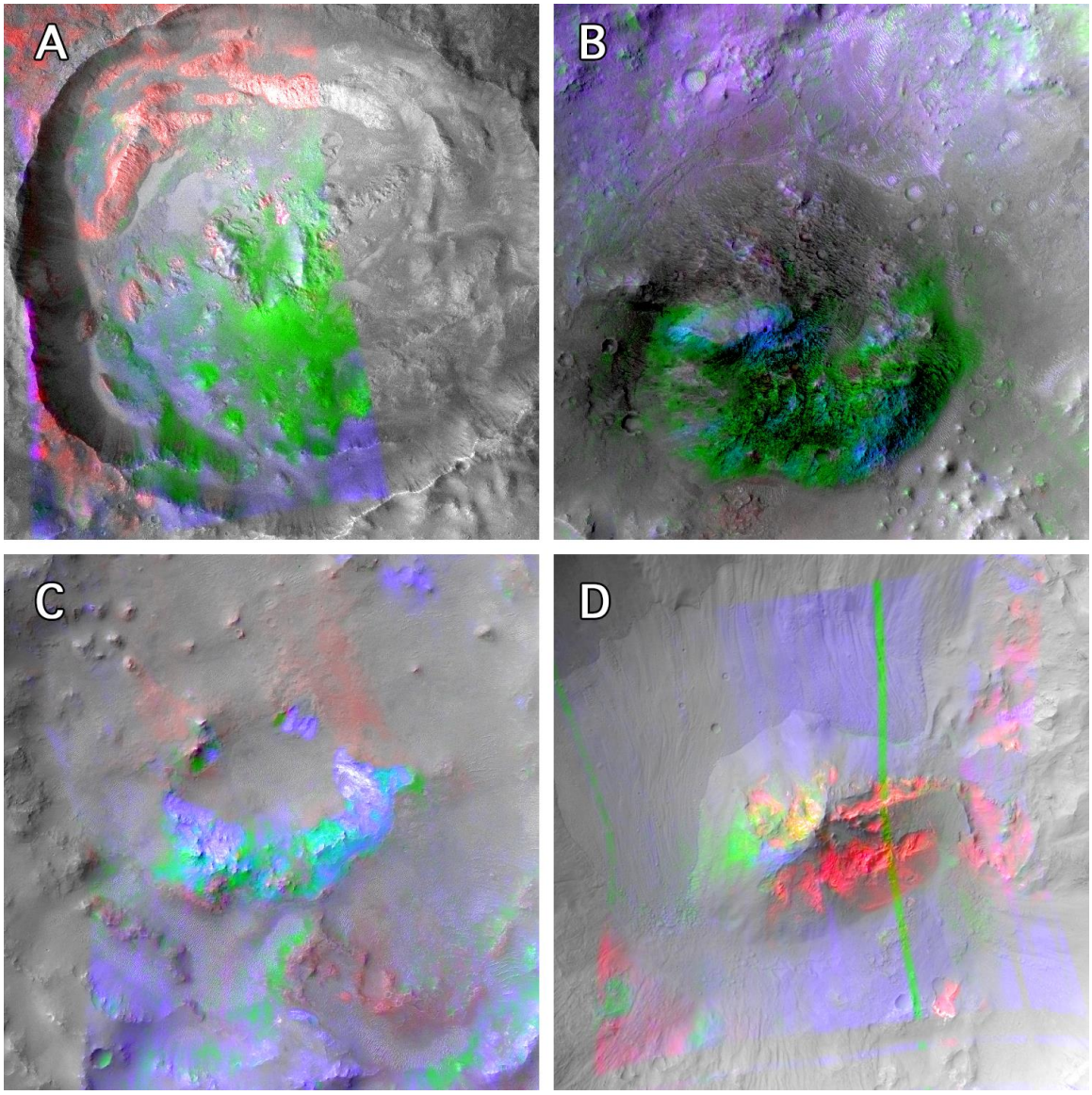

Figure S1. CRISM maps of modeled mineralogy projected over CTX imagery (same parameters as Figure 1). A: Taytay Crater (CRISM ID: HRL00005B77). B: Balvicar Crater (FRT0001FBC1). C: Unnamed crater (FRT00017B42). D: Unnamed crater (CRISM ID: FRT0001EBA0).

Modeling details: Endmember selection

We used a variety of mafic materials as spectral endmembers in our unmixing model (Table S1). Most of these spectra are publically available in the RELAB database (http://www.planetary.brown.edu/relabdata/data/); the mafic glass spectrum is available by request.

Table S1. Spectral endmembers used in the unmixing model

Endmember description	**RELAB ID**
Synthetic orthopyroxene Wo0En80Fs20	DL-CMP-002
Synthetic orthopyroxene Wo0En50Fs50	DL-CMP-004
Synthetic pigeonite Wo14En36Fs50	DL-CMP-011
Synthetic clinopyroxene Wo25En36Fs39	DL-CMP-057
Synthetic clinopyroxene Wo39En36Fs25	DL-CMP-073
Olivine (Fo_{68}) from Chassigny	DD-MDD-001
St. Peter's Fayalite	PO-CMP-071
Synthetic mafic glass	–
CRISM column mean	–
Shade (w=0)	–
Bright (w=1)	–
-1 slope	–

The CRISM column mean is the mean spectrum from the entire detector column (one 'sample' of the unprojected CRISM scene) for a given pixel. This endmember likely contains mafic components; so mixing it with laboratory endmembers precludes us from determining absolute mineral abundances (Goudge et al., 2015). However, by doing this we are confident the resulting modeled mineral signatures are actually present and are not

simply fitting the background continuum shape of the CRISM scene. The shade endmember is physically represented by opaque minerals and actual shade in the scene, the bright endmember by visible/near-infrared neutral minerals like plagioclase, and the -1 slope by leached rinds on glass discussed in detail by Minitti et al. (2007), and used in previous modeling of martian remote sensing data (Combe et al., 2008).

Data processing

CRISM data were systematically processed (Murchie et al., 2009) by dividing by the cosine of the solar incidence angle, and absorptions due to atmospheric gases were then removed by scaling an empirical atmospheric transmission spectrum to each CRISM pixel observation using the volcano scan method (Murchie et al., 2009). Only the L-detector data from 1.021-2.497 μm were used for spectral mixture modeling.

Spectral modeling details

The Hapke model is an approximate solution to the radiative transfer equation (Chandrasekhar, 1960) that estimates the reflectance of a semi-infinite particulate surface. In this model the radiance coefficient r_c is given (Hapke, 1981) as:

$$r_c = \frac{w}{4}\frac{1}{\mu_0 + \mu}\{[1 + B(g)]P(g) + H(\mu_0)H(\mu) - 1\}$$

where μ_0 and μ are the cosine of the incidence and emission angles, respectively, B() is the backscattering function, P() is the phase function, g is the phase angle, and H() is an approximation to the H-function from Hapke (1981), given (Hapke, 2002) as:

$$H(x) \approx \left[1 - wx(r_0 + \frac{1 - 2r_0 x}{2} \ln\left\{\frac{1+x}{x}\right\}\right]$$

where:

$$r_0 = \frac{1-\gamma}{1+\gamma}$$

and

$$\gamma = \sqrt{1-w}$$

Single-scattering albedo describes the ratio of the scattering efficiency Q_S of a particle to its extinction efficiency Q_E (scattering plus absorption). We used a lookup table built from the above equations to convert endmember reflectance spectra and CRISM data to single-scattering albedo, assuming B(g) = 0 and P(g) = 1. These simplifying assumptions have been proven to be valid for a variety of laboratory and planetary applications (Mustard and Pieters, 1989; Goudge et al., 2015) for the intermediate phase angles that the CRISM data were acquired at.

In single-scattering albedo space, endmember components in a mixture combine linearly (Hapke, 1981):

$$w_{mixture} = \sum_{i=1}^{n} F_i w_i$$

where F_i is the relative geometric cross-section of each component *i*:

$$F_i = \frac{\frac{M_i}{\rho_i D_i}}{\sum_i^n \left\{\frac{M_i}{\rho_i D_i}\right\}}$$

and M_i, ρ_i, and D_i are the bulk density, solid density, and particle diameter, respectively. Because we are not concerned with absolute abundances in this study and because particle size is not solved for, we take F to be the relative spectral contribution of an endmember to the mixture and do not attempt to calculate mass or volumetric fractions of endmembers.

We used the linear least-squares *lsqlin* function in Matlab with a medium-scale active set algorithm to invert each CRISM pixel (converted to single-scattering albedo) into the spectral fraction F of each endmember. Example code for this procedure is:

[*F*,*SSE*] = lsqlin(*endmembers*,*unknownSpectrum*,[],[],ones(1,M),1,zeros(1,M))

Where *endmembers* is an N×M matrix of M endmember spectra with N spectral channels, *unknownSpecrum* is the N×1 CRISM spectrum vector, *F* is the M×1 vector output for the fraction of each endmember, and *SSE* is the root mean square error. The code above imposes that no endmember can have a negative F value, and that $\sum F_i = 1$ (non-negativity and sum-to-one constraints).

We run the model without and with mafic glasses, then perform an F-test to determine if adding a mafic glass endmember improves the model fit at the 99% confidence level by calculating the F-test value:

$$Ftest = \left\{\frac{SSE_K - SSE}{(M-K)SSE}\right\}(N-K-1)$$

Where SSE_K and SSE are the values without and with mafic glass in the endmember suite, respectively. M is the number of endmembers including mafic glass, K the number of endmembers without mafic glass (therefore M-K =1), and N is the number of spectral

channels. For each pixel, if the calculated F-test value is not greater than the critical F value at α=0.01 then we use the model solution with no mafic glass present.

Model Validation

We benchmarked our spectral modeling approach against physical laboratory mixing studies. First, we replicated the three-component mixtures of anorthite, enstatite and olivine from Mustard and Pieters (1987), using their three actual endmember spectra and adding: our basaltic glass spectrum, w=0, w=1, and -1 slope endmembers (Table S2). We clipped the spectra to the same wavelength range used for modeling CRISM data. These laboratory measurements had a spectral sampling of 10 nm, lower than that of CRISM.

Table S2. Validation of unmixing model against Olivine-Enstatite-Anorthite laboratory mixtures, where meas = measured abundance, mod = modeled abundance, and norm = normalized abundance after removing albedo and slope-modifying endmembers.

	Mix 1	**Mix 2**	**Mix 3**	**Mix 4**	**Mix 5**	**Mix 6**	**Mix 7**
Olivine$_{meas}$	**0.6527**	**0.1541**	**0.1414**	**0.4061**	**0.1501**	**0.3848**	**0.3106**
Enstatite$_{meas}$	**0.1579**	**0.6574**	**0.1405**	**0.4062**	**0.3851**	**0.1488**	**0.3097**
Anorthite$_{meas}$	**0.1894**	**0.1884**	**0.7181**	**0.1878**	**0.4647**	**0.4664**	**0.3797**
Olivine$_{mod}$	0.6519	0.1500	0.1410	0.4008	0.1483	0.3883	0.3087
Enstatite$_{mod}$	0.1649	0.6724	0.1470	0.4205	0.4009	0.1565	0.3229
Anorthite$_{mod}$	0.1735	0.1672	0.7087	0.1652	0.4410	0.4473	0.3566
Glass$_{mod}$	-3.17E-19	6.64E-19	2.64E-19	-4.21E-19	6.49E-19	-3.09E-19	-3.84E-19
w=0$_{mod}$	-7.71E-19	-3.33E-19	-1.63E-19	-1.09E-18	-3.63E-19	-6.56E-19	-9.62E-19
w=1$_{mod}$	0.0097	0.0104	0.0032	0.0135	0.0099	0.0080	0.0117

-1 $slope_{mod}$	1.43E-19	1.94E-19	5.17E-20	1.96E-19	1.59E-19	1.17E-19	1.70E-19
$Olivine_{norm}$	**0.6583**	**0.1516**	**0.1415**	**0.4063**	**0.1497**	**0.3914**	**0.3124**
$Enstatite_{norm}$	**0.1665**	**0.6795**	**0.1475**	**0.4263**	**0.4049**	**0.1577**	**0.3268**
$Anorthite_{norm}$	**0.1752**	**0.1689**	**0.7110**	**0.1674**	**0.4454**	**0.4509**	**0.3609**
<Abs. Diff>	0.0095	0.0147	0.0047	0.0136	0.0132	0.0104	0.0126

These results show that the model is able to accurately determine relative mineral fractions in multi-component mafic mixtures, and determine absolute abundances to within ~1% when the exact endmember spectra are available. Importantly it does not model glass when it is not present, and adding in w=0, w=1 and -1 slope endmembers does not significantly affect the results.

We then performed new physical mixture experiments of four powdered mafic/ultramafic terrestrial samples spiked with varying amounts of a synthetic mafic glass. We used the same spectral endmember library as in our study (Table S1), with none of the endmembers being derived from the actual samples (a different mafic glass was used). This provides a more robust test than the 3-component mixture above, because no *a priori* information about the minerals in the sample is incorporated into the model. We found that detection limits for mafic glass were ~10 wt. %. When we included the spectra of the pure rocks themselves as an endmember, the relative spectral fractions of mafic glass accurately reflected the relative abundance of glass in the mixtures (Table S3). This is analogous to using the CRISM column mean as an endmember when modeling CRISM data: essentially, including this kind of "in-scene" endmember accounts for much of the spectral signature of the mixture, and the remaining signal is

more accurately modeled in terms of its mineralogy. Again, mafic glasses were not modeled at all when they were not present in the samples.

Table S3. Modeled glass abundances for four terrestrial rocks spiked with 0, 5 and 10 wt. % mafic glass, when using the pure rock as a spectral endmember. While absolute abundances differ between samples, relative modeled abundances are quite accurate.

	Bushveld pyroxenite	**Bushveld norite**	**Cyprus Ol-rich basalt**	**San Carlos dunite**
Glass 0_{mod}	0	0	0	0
Glass 5_{mod}	0.0244	0.0139	0.0235	0.0377
Glass 10_{mod}	0.0543	0.0321	0.0449	0.0788
$Ratio_{meas}$	2	2	2	2
$Ratio_{mod}$	2.23	2.31	1.91	2.09

References

Chandrasekhar, S., *Radiative Transfer* (Dover Publications, New York, 1960).

Combe, J.-Ph., et al., 2008, Analysis of OMEGA/Mars Express data hyperspectral data using a Multiple-Endmember Linear Spectral Unmixing Model (MELSUM): Methodology and first results: Planetary and Space Science, v. 56, p. 951-975, doi:10.1016/j.pss.2007.12.007.

Goudge, T.A, Mustard, J.F., Head, J.W., III, Salvatore, M.R., and Wiseman, S.M., 2015, Integrating CRISM and TES Hyperspectral Data to Characterize a Halloysite-Bearing Deposit in Kashira Crater, Mars: Icarus, v. 250, p. 165-186, doi: 10.1016/j.icarus.2014.11.034.

Hapke, B., 1981, Bidirectional Reflectance Spectroscopy I. Theory: Journal of Geophysical Research, v. 86, p. 3039-3054, doi:10.1029/JB086iB04p03039.

Hapke, B., 2002, Bidirectional Reflectance Spectroscopy 5. The Coherent Backscatter Opposition Effect and Anisotropic Scattering: Icarus, v. 157, p. 523-534, doi:10.1006/icar.2002.6853.

Minitti, M.E., Weitz, C.M., Lane, M.D., and Bishop, J.L., 2007, Morphology, chemistry, and spectral properties of Hawaiian rock coatings and implications for Mars: Journal of Geophysical Research, v. 112, E05015, doi:10.1029/2006JE002839.

Murchie, S.L., et al., 2009, Compact Reconnaissance Imaging Spectrometer for Mars investigation and data set from the Mars Reconnaissance Orbiter's primary science phase: Journal of Geophysical Research, v. 114, E00D07, doi:10.1029/2009JE003344.

Mustard, J.F., and Pieters, C.M., 1989, Photometric Phase Functions of Common Geologic Minerals and Applications to Quantitative Analysis of Mineral Mixture Reflectance Spectra: Journal of Geophysical Research, v. 94, p .13619-13634, doi:10.1029/JB094iB10p13619.

Mustard, J.F., and Pieters, C.M., 1987, Quantitative Abundance Estimates from Bidirectional Reflectance Measurements: Journal of Geophysical Research, v. 92, E617-E626, doi: 10.1029/JB092iB04p0E617.